https://doi.org/10.52131/jmps.2024.0501.0042

Journal of Materials and Physical Sciences

Volume 5, Number 1, 2024, Pages 10 - 19

Journal Homepage:
https://journals.internationalrasd.org/index.php/jmps

JOURNAL OF MATERIALS AND PHYSICAL SCIENCES
INTERNATIONAL RESEARCH ASSOCIATION FOR SUSTAINABLE DEVELOPMENT

Transport Properties of Ternary $KAlTe_2$ and $KInTe_2$ Using Density Functional Theory

Qasimullah[1*], Zeshan Javed[2], Basit Saeed Khan[3], Gulfam Nasar[4], Ghulam Farid[5,6]

[1] Faculty of Physical and numerical sciences, Qurtuba university of science and information technology Peshawar 25100, Pakistan
[2] Institute of Physics, The Islamia University of Bahawalpur, Bahawalpur, 63100, Pakistan
[3] Polymer Physics Laboratory, Institute of Physics, Bahauddin Zakariya University, Multan 60800, Pakistan
[4] Department of Chemistry, Balochistan University of Information Technology, Engineering & Management Sciences, Quetta 87300, Pakistan
[5] Department of Applied Physics, University of Barcelona, C/Martí i Franquès, 1, 08028, Barcelona, Catalunya, Spain
[6] ENPHOCAMAT Group, Institute of Nanoscience and Nanotechnology (IN2UB), University of Barcelona, C/ Martí i Franquès, 1, 08028, Barcelona, Catalunya, Spain

ARTICLE INFO

Article History:
Received: March 24, 2024
Revised: April 04, 2024
Accepted: June 27, 2024
Available Online: June 30, 2024

Keywords:
Electronic Nature
Thermoelectricity
Anisotropy
DFT
Boltzmann's Theory

ABSTRACT

The anisotropic ternary $KAlTe_2$ and $KInTe_2$ materials have been investigated using Density Functional Theory. The energy of these material is optimized to its ground state, and this data is subsequently compared with the current theoretical and experimental literature. Our results reveal that $KAlTe_2$ exhibits a direct band gap of 1.68 eV, while $KInTe_2$ demonstrates a calculated band gap of 0.931 eV. The semi classical Boltzmann method, implemented through the BoltzTraP package, was used to assess the key thermoelectric characteristics, including thermal conductivity, the Seebeck coefficient, figure of merit (ZT). The Seebeck coefficient is measured at -11.99 μV/K, whereas for the material $KInTe_2$, it ranges from 11.96 μV/K to 8.08 μV/K within the energy range of 0.00 eV to -0.02 eV. In the N-type region, the highest Seebeck coefficient values for $KAlTe_2$ and $KInTe_2$ materials are recorded -0.35 to -0.57 μV/K and 5.5 to 6.7 μV/K, respectively.

*Corresponding Author's Email: qasimullah9966@gmail.com

1. Introduction

There is a significant demand for emerging semiconductors possessing the right physical properties to meet the demands of upcoming electronic devices and products. Semiconductors that facilitates the flow of various non-toxic chemical elements are of great interest to physicists, chemists, and material scientists alike. Three presents elements that are members of the periodic table make up the current system, which has an A-B-X_2 structure. In this arrangement, group element A is the first. Alkali metals" is known as the 1st group of elements, where "B" refers to elements from the 3rd group placed in the periodic table, where as "X" denotes to chalcogenide elements placed in the 6th group. The chemical structures of $KAlTe_2$ and $KInTe_2$ are typically regarded as the most stable within the context of the A-B-X system's physical-chemical interactions (Belgoumri et al., 2018; Benmakhlouf et al., 2015; Benmekideche et al., 2018; Bouchenafa et al., 2020).

In the late 1900s, the $KAlTe_2$ and $KInTe_2$ materials stoichiometry were first exploited and it was found the materials show relative instability and highly challenging to synthesize pure composites as the alkali metals' possess a higher chemical reactivity (Benmakhlouf et al., 2015; Kim & Hughbanks, 2000; Range & Mahlberg, 1975; Saeed, Ali, et al., 2022;

Saeed et al., 2019; Schubert & Hoppe, 1970; Weis, Schäfer, & Schön, 1976). The $KAlTe_2$ and $KInTe_2$ system materials have been the hot topic of various experimental literature, in the late 2000s because of its distinct characteristics (Isaenko et al., 2003; Saeed, Noor, et al., 2021; Saeed, Uddin, et al., 2021). Semiconductors make up majority of ternary chalcogenides with the formula $KAlTe_2$ and $KInTe_2$. The majority of ternary chalcogenides with the chemical formula $KAlTe_2$ and $KInTe_2$ have semiconductor characteristics, with band gaps ranging from 0.9 eV to 4.0 eV (Weis et al., 1976). Zoltan et al., extensively investigate the crystallographic categorization of the $KAlTe_2$ and $KInTe_2$ complexes (Isaenko, Vasilyeva, Merkulov, Yelisseyev, & Lobanov, 2005).

For the first time in 1972, Franke et al., employed the Weissenberg photographic technique to successfully index the tetragonal unit cell and developed predictable atomic coordinates. They reported the single-crystal structure, precise bond distances and angles of these concern materials. Single crystals were generated at a temperature of 1275 K through a reaction involving the target composition. The crystal-growth experiment was executed by employing a eutectic halide flux, in accordance with a method that had been previously documented (Bouchenafa et al., 2020; Fu et al., 2014).

The discovery of Franke and Schafer revealed that these compounds form a tetragonal crystalline system, with determinable atomic positions. Two decades later, Hung and Hwu provided additional information into the bond lengths present within the single crystals. In 1976, Weis provided the structural characteristics of the tetragonal ternary compound. Although a lot of literature is available on the above mentioned materials, however, several fundamental physical aspects of it remain unexplored, just like thermoelectric and mechanical properties (Perdew et al., 2008; Ward, Pozzi, Van Duyne, & Ibers, 2014). Therefore, in this manuscript, the semi-classical Boltzmann method was applied to the BoltzTraP package, enabling the determination of thermoelectric properties such as thermal conductivity, the Seebeck coefficient, thermal conductivity and figure of merit (ZT).

The Seebeck Coefficient for $KInTe_2$ ranges from 11.96 μV/K to 8.08 μV/K within the energy range of 0.00 eV to -0.02 eV, whereas $KAlTe_2$ exhibits a Seebeck Coefficient of -11.99 μV/K. In the N-type region, the maximum Seebeck Coefficients for these materials are -0.35 to 0.57 μV/K for $KAlTe_2$ and 5.5 to 6.7 μV/K for $KInTe_2$, respectively.

2. Method of Calculations

The density functional theory (DFT) framework, in combination with the full-potential Linearized Augmented Plane Wave (FP-LAPW) method, has been implemented using the WIEN2k package (Fabiano, Constantin, & Sala, 2011), to examine the electronic nature of $KAlTe_2$ and $KInTe_2$. In order to determine the structural features, the local density approximation (LDA) was used to represent the exchange-correlation energy (Morrison, 2019) and the generalized gradient approximation of Perdew et al. (Gerolin, Grossi, & Gori-Giorgi, 2019). Conventional GGA and LDA functional tend to overestimate the energy band gap of semiconductor and insulator materials, while compared to similar observed values. In order to solve the significant issue of underestimating the band gap, certain functional based on GGA and LDA approaches have been developed to provide improved representations of the electronic structures in semiconductors and insulators.

The magnetic and thermoelectric properties of the studied system manifest as the generation of voltage when two junctions, comprised of dissimilar conductors or semiconductors, are maintained at varying temperatures ΔT, leading to the flow of electrical current. This production of this thermoelectric power is the outcome of the Seebeck effect. The equation $\Delta V = (S)\Delta T$ defines the open-circuit potential difference ΔV, where "S" denotes the Seebeck coefficient, measured in V.K-1. This coefficient represents the magnitude of the generated voltage in response to the temperature gradient across the material. The assessment of a material's thermoelectric performance is determined through the dimensionless thermoelectric figure of merit (ZT), which is calculated as $ZT = S^2T(\sigma/\kappa)$. The thermoelectric coefficients were determined by solving the Boltzmann transport properties using a constant relaxation time, the rigid band approximation, and first-principles calculations (Gerolin et al., 2019).

3. Results and Discussion

3.1. Band Structure

While the band gap of the materials can be roughly estimated from the density of states plots, their specific band gap nature (e.g., whether it is direct or indirect) remains undisclosed. The band structure results discussed in the literature for investigated compounds showed direct band semiconductors nature (Gori-Giorgi & Baerends, 2018; March & Angilella, 2016; Mardirossian & Head-Gordon, 2016; Xiaoying, 2020). As depicted in Figure 1, the band structure profile generated using GGA allows for the precise determination of both the magnitude and characteristics of the band gap. This data suggests that all these compounds meet the criteria for being direct band semiconductors, as their lowest and highest conduction bands align with the Γ- and R symmetry points. Figure 1 illustrates the results of The Fermi energy stage at 0.0 eV serves as a reference point to facilitate our comprehension of the electrical properties of $KAlTe_2$ and $KInTe_2$. The precise alignment of the conduction band minima and valence band maxima for $KAlTe_2$ within the first Brillouin zone strongly suggests that the material exhibits the characteristics of a direct band gap semiconductor. These materials display semiconducting properties due to the intricate associated symmetrical components of R, Γ, X, and M. Similarly, $KInTe_2$, has a band structure, denoting the semiconductor characteristics since the valence band states are not crossing the Fermi levels. The analysis of the Γ and R points indicates that both of the studied compounds exhibit characteristics of indirect band gap semiconductors. The computed band gap values for $KAlTe_2$ and $KInTe_2$ are 1.68 eV and 0.931 eV, respectively. Dropping of the bandgap value is associated with the primary factor of Al atoms being replaced with in atoms. $KInTe_2$ offers an opportunity of being utilized in solar cells due to its exciting narrow band gap to enhance absorption, while on the other hand, $KAlTe_2$ could be employed in other photovoltaic devices demanding less absorption or high transparency, such as light emitting diodes, according to comparisons of the band gaps.

3.2. Density of States

Figure 2 illustrates that the density of states graphs, where the valance band is represented by the negative energy levels, the conduction band by the positive energy states, and E_f represents the Fermi energy level, coinciding with the zero-energy state of the valence band's edge. The energy band gap is the distance between valance band's margins and the conduction band minimum. One may determine if a material is metallic, semiconductor, or an insulator based on the size of this band gap. From the Figure 2, one can see that all $KAlTe_2$ and $KInTe_2$ are indirect band gap semiconductors, with the aid of the GGA potential approach in DFT (Perdew et al., 2008). Where the valence and conduction band edges are contributed by (Al/In) and K for both materials. Consequently, the electronic properties of these compounds are mostly determined by the electronic properties of (Al/In) and K. The Density of state plots of the compounds $KAlTe_2$ and $KInTe_2$ demonstrate that these compounds could prove to be effective thermoelectric materials as the intense peaks near the valence band edge correlate with elevated carrier concentration. This insight is extracted from the partial density of states graphs presented in Figure 2, enabling us to comprehend the occurrence frequency of each state within the atom's valence and conduction bands (Dipsey, 2016; Moltved & Kepp, 2019; Xie, Wu, & Zhao, 2021). The total density of states diagrams in Figure 2 do not provide clarity on which atomic states of Al/In and K are contributing to the edges of the conduction and valence bands. Graphs depicting the TDOS and PDOS of the tetragonal ternary crystal are presented. Figure 2 exhibits the outcomes of the DOS and PDOS calculations for $KAlTe_2$. The range spans from -6 eV to 6 eV.

Among the contributing orbitals, Te-d, K-d, and Al-d exhibit minimal influence, while Te-pz and Al-s dominate the contributions below the Fermi energy level. The Te-px orbital makes a negligible contribution to the conduction band. Figure 2 presents the DOS and PDOS plots for $KInTe_2$, covering an energy range from -6 eV to 6 eV. It's noteworthy that Te-p and K-pxpy orbitals contribute significantly below the Fermi energy level, while K-p, In-pz, and In-px+py orbitals make a smaller contribution.

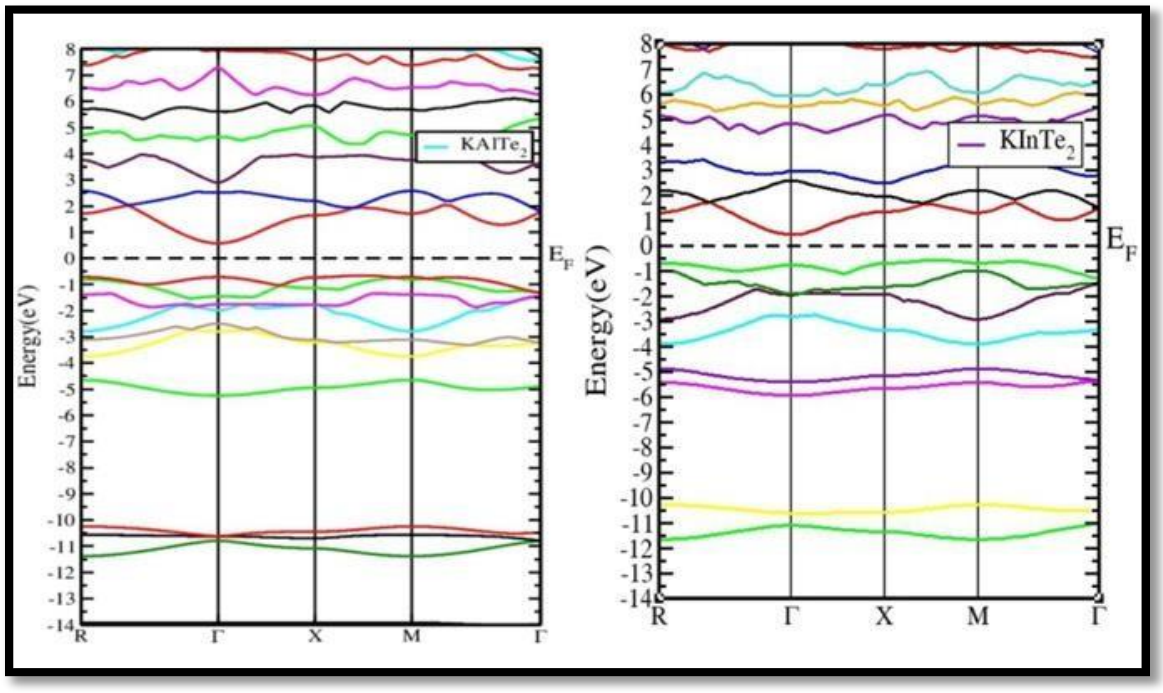

Figure 1: The Band structure of $KAlTe_2$ and $KinTe_2$ by applying GGA potential

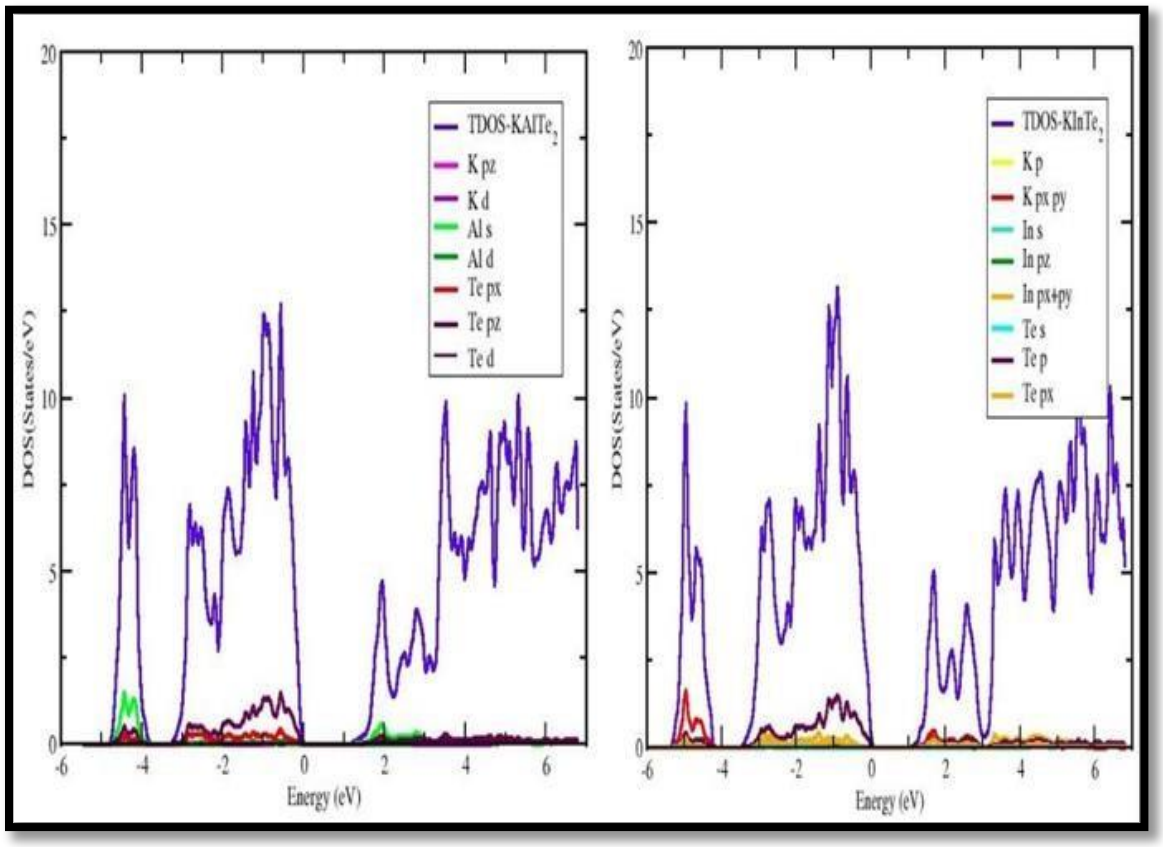

Figure 2: The TDOS and PDOS of $KAlTe_2$ and $KInTe_2$ in non-spin calculation

3.3. Seebeck Coefficient

Thermoelectric phenomenon is incomplete if a person unable to grasp the knowledge about Seebeck coefficient, which holds fundamental significance. With the help of Seebeck coefficient, induced voltage amount caused by a temperature differential can be calculated. The SI unit for Seebeck Coefficient is volt per kelvin. A substance with a large magnitude value is produces and controls thermoelectric energy. While N-doped materials exhibit a negative Seebeck coefficient, P-doped materials demonstrate a positive coefficient (Claeys

et al., 2020; Ikeda et al., 2019; Saeed, Haq, et al., 2022). The chemical potential is the proportion of a material's charge carrier concentration to its doping level. One of the essential components for improving thermoelectric characteristics is assumed to be chemical potential (Kaur & Sinha, 2021). The figures illustrate the relationship between the Seebeck coefficient and the chemical potential (μ) for tetragonal ternary materials. Figure 3(a, b) further illustrates that the Seebeck coefficient values for KAlTe2 and KInTe2 within the chemical potential (μ) range of -0.01 eV to 0.00 eV are 8.06 μV/K and -11.99 μV/K, respectively, and within the range of 0.00 eV to -0.02 eV for KInTe2, the values are 11.96 μV/K and 8.08 μV/K. In the specific regions where a high value of the Seebeck coefficient is attained. The maximum Seebeck Coefficient values for the materials $KAlTe_2$ and $KInTe_2$ in the N-type region are -0.35-0.57 μV/K and 5.5-6.7 μV/K, respectively. As indicated by Figure 3(a, b), both materials exhibit high Seebeck coefficient values in close proximity to the Fermi energy within the N- and P-type regions. The Seebeck coefficient values for $KAlTe_2$ are more pronounced in the vicinity of the N-type, suggesting a predominance of N-type doping, in contrast to $KInTe_2$ where P-type doping is more prevalent. The Seebeck coefficient exhibits a significantly higher value in the P-type region as compared to the N-type region, highlighting the prevalence of P-type doping in these materials.

3.4. Electrical Conductivity per Relaxation Time (σ/τ)

The electrical conductivity of the material is utilized to assess its thermoelectric properties. The electrons and holes both contribute to conductivity. In conductors, electrons contribute to current, while in semiconductors, both holes and electrons play a role in conducting current (Baira, Siad, & Siad, 2021; S. Feng et al., 2021). Given that the material under study is a semiconductor, it's the movement of electrons and holes that generates the current. Figure 4(a, b) presents the relationship between electrical conductivity per relaxation time (σ/τ) and chemical potential for the materials of interest. It also demonstrates that, in both P-type and N-type materials, (σ/τ) is more pronounced in the heavily doped region and maintains a value of zero at the Fermi level. In the case of $KAlTe_2$ and $KInTe_2$, as shown in the figure, (σ/τ) is greater for N-type materials when compared to P-type materials. In the P-type category, the maximum values for $KAlTe_2$ and $KInTe_2$ are 3.18 to 3.81 × 10^20 1/Ωms and 4349 to 1905 × 10^20 1/Ωms, respectively. The N-type values for KAlTe2 and KInTe2 amount to 0.9 to 3.5 × 10^20 1/Ωms and 2946 to 3208 × 10^20 1/Ωms, respectively.

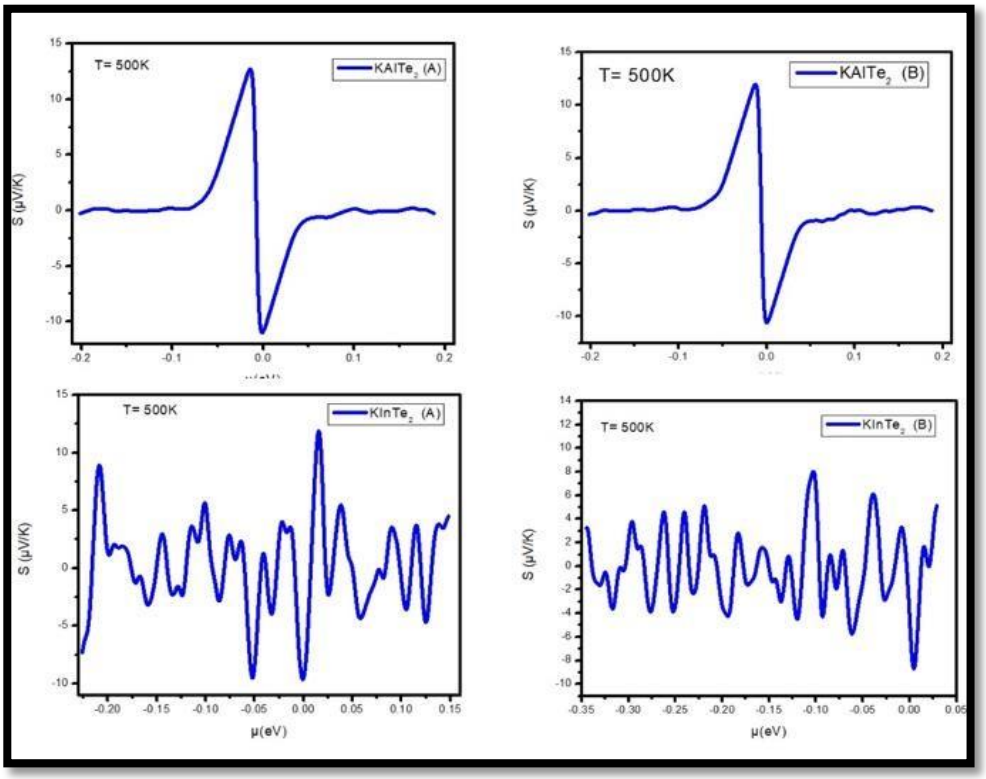

Figure 3(a, b): The Seebeck coefficient plotted against the chemical potential for $KAlTe_2$ and $KInTe_2$

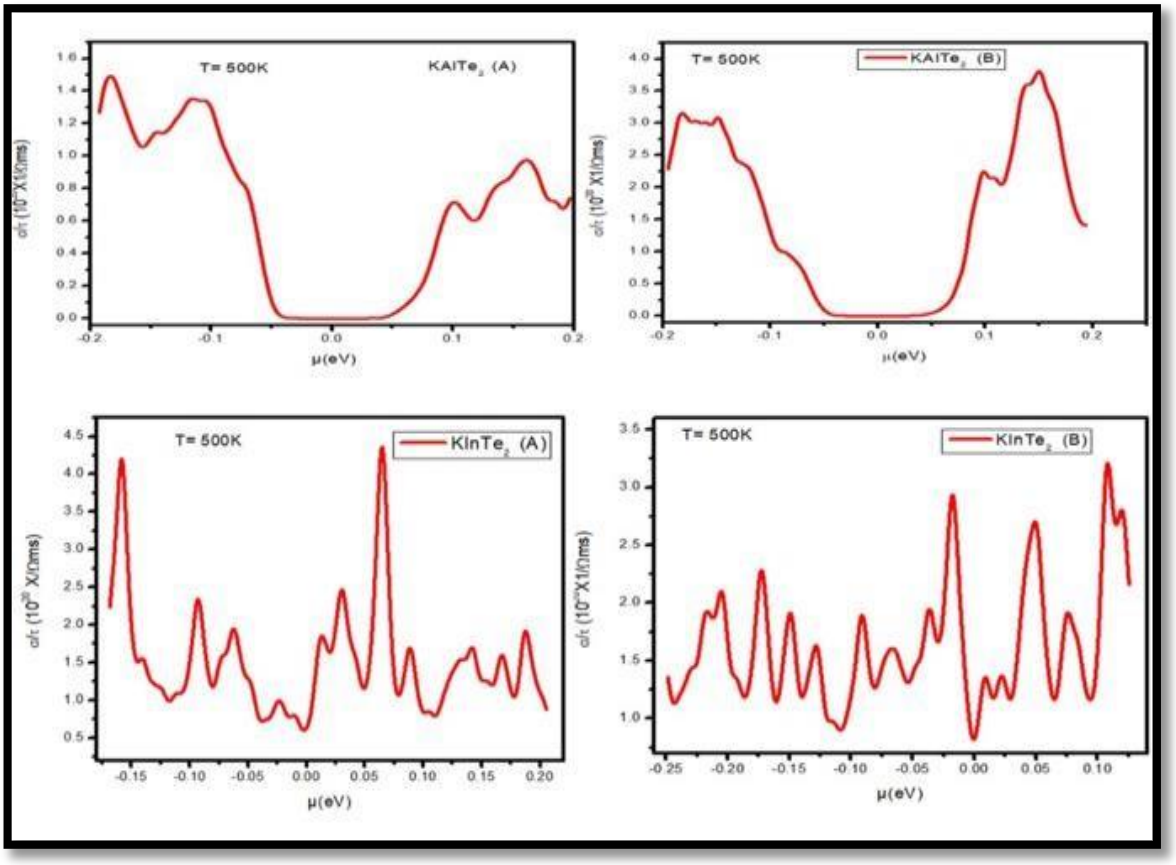

Figure 4(a, b): The electrical conductivity per relaxation time of $KAlTe_2$ and $KInTe_2$ in relation to the chemical potential at a temperature of 500K

Table 1
The Seebeck coefficient of the materials of interest, with 'P' representing P-type and 'n' for Ntype semiconductors

Material	XX=YY(A) μV/K	ZZ(B) μV/K	Temperature (K)	Chemical Potentialμ(eV) XX=YY(A)	Chemical Potentialμ(eV) ZZ(B)
$KAlTe_2$ (XX=YY, ZZ) (XX=YY=A, ZZ=B)	P=1282.4 N=0.35	P=11.99 N=0.57	500	P=-0.01 to -0.00 N=0.0-0.2	P=0.00-(-0.02) N=0.0-0.02
KInTe2 (XX=YY, ZZ) (XX=YY=A, ZZ=B)	P=11.96 N=5.5	P=8.08 N=6.7	500	P=-0.02 to -0.00 N=0.0-0.2	P=0.00-(-0.02) N=0.0-0.02

Table 2
The electrical conductivity of the materials of interest, with 'P' denoting P-type and 'n' for N type semiconductors

Material	XX=YY(A) 10^{20}1/Ωms	ZZ(B) 10^{20}1/Ωms	Temperature (K)	Chemical Potentialμ(eV) XX=YY(A)	Chemical Potentialμ(eV) ZZ(B)
$KAlTe_2$ (XX=YY, ZZ) (XX=YY=A, ZZ=B)	P=3.18 N=3.81	P=3.9 N=4.9	500	P=-0.01 to -0.00 N=0.0-0.2	P=0.00-(-0.02) N=0.0-0.02
$KInTe_2$ (XX=YY, ZZ) (XX=YY=A, ZZ=B)	P=4349 N=1905	P=2946 N=3208	500	P=-0.02 to -0.00 N=0.0-0.2	P=0.00-(-0.02) N=0.0-0.02

3.5. Electronic Thermal Conductivity per Relaxation Time (κ/τ)

Thermal conductivity is significantly affected by the presence of electron-hole pairs in semiconductor materials. it can be expressed as $k = k_e + k_h$, where ke is associated with electron vibrations, and k_h corresponds to hole vibrations. In semiconductors, thermal

conductivity is attributed to electron-hole pairs, while in metals, it's predominantly driven by free charge carriers or electrons (Hausmann, Oudah, Ikeda, Yonezawa, & Maeno, 2018; Yuan et al., 2021). Figure 5(a,b) illustrates the correlation between thermal conductivity per relaxation time (κ/τ) and chemical potential for the two materials. The chemical potential increases from the Fermi level, which is at 0 μ(eV), up to (κ/τ), as depicted. In both the P-type and N-type regions, the chemical potential (κ/τ) is in full effect (Y. Feng et al., 2019).

In P-type region of $KAlTe_2$ is 16.21 to 37.6×10^{14}W/mKs while for $KInTe_2$is 35204 to 2175510^{14}W/mKs. Numerical value for N-type is 11.28 to 46.3×10^{14}W/mKs, and 29.65 to 34.92×10^{14}W/mKs, respectively.

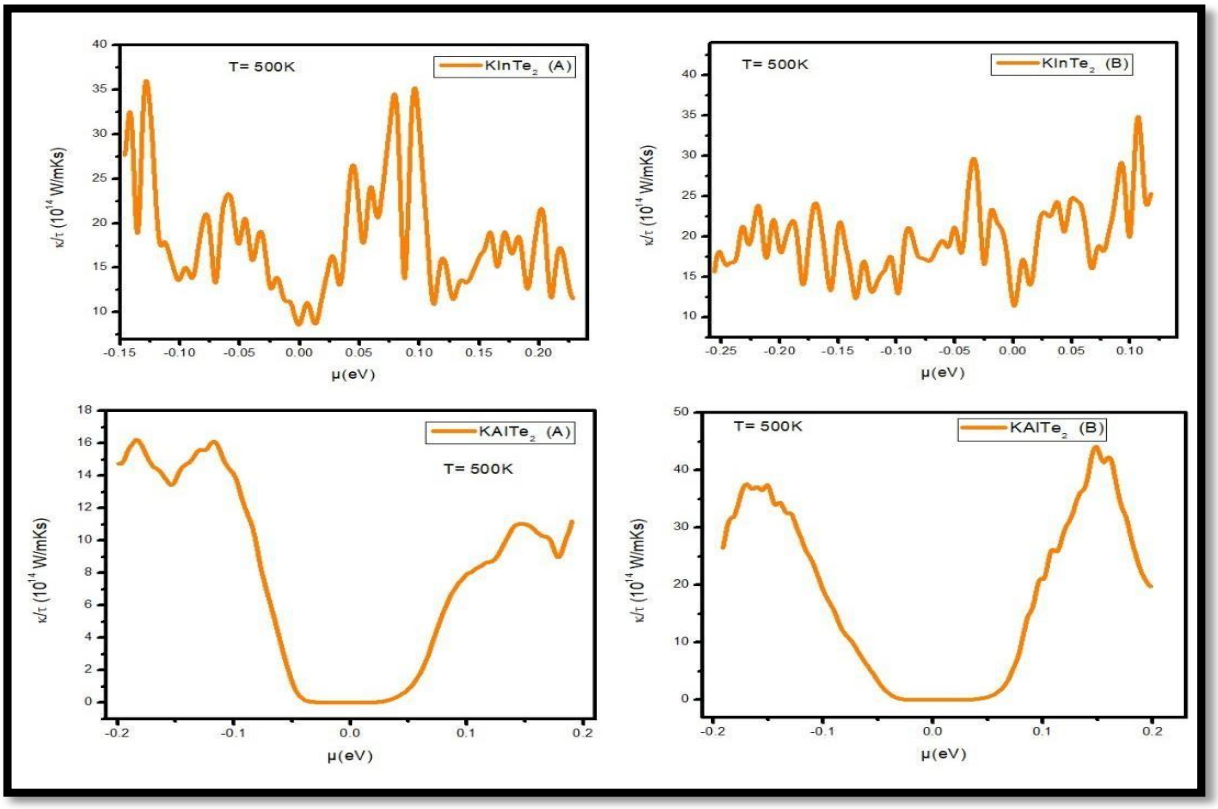

Figure 5(a, b): The Electronic Thermal Conductivity for $KInTe_2$ and $KAlTe_2$ against the chemical potential

Table 3
The thermal conductivity of the materials of interest, with 'P' representing P-type and 'n' for N type semiconductors

Material	XX=YY(A) 10^{14}W/mKs	ZZ(B) 10^{14} W/mKs	Temperature (K)	Chemical Potentialμ(eV) XX=YY(A)	Chemical Potentialμ(eV) ZZ(B)
$KAlTe_2$ (XX=YY, ZZ) (XX=YY=A, ZZ=B)	P=4394 N=0.35	P=11.99 N=0.57	500	P=-0.01 to -0.00 N=0.0-0.2	P=0.00-(-0.02) N=0.0-0.02
$KInTe_2$ (XX=YY, ZZ) (XX=YY=A, ZZ=B)	P=35204 N=21755	P=29.65 N=34.92	500	P=-0.02 to -0.00 N=0.0-0.2	P=0.00-(-0.02) N=0.0-0.02

3.6. Figure of Merit

Utilizing the figure of merit parameter (ZT), one can evaluate the thermoelectric properties, such as the Seebeck coefficient, thermal conductivity, and electrical conductivity of the given materials. The equation $ZT= S^2T\sigma /\kappa$ indicates that ZT values will be substantial when both S and σ values are elevated, while the value of κ remains low (Y. Feng et al., 2019). The plot of ZT against the chemical potential for Tetragonal $KAlTe_2$ and $KInTe_2$ are presented in figure 6 (a, b). The peak ZT values for $KAlTe_2$ and KInTe2 fall within the range of 0 eV to 0.02 eV for both (a) and (b), respectively. An increasing trend in (ZT) is noticeable throughout the entire compound within the N-type region as opposed to the P-type region. Nevertheless, this behavior signifies a significant response of (ZT) for the N-type configuration. To achieve optimal thermoelectric performance, materials should

possess ZT values equal to or exceeding 1 (Hardianto, 2020; Sofi & Shah, 2019). From the figure, the peak value of ZT for $KAlTe_2$ and $KInTe_2$ are 0.99 and 1.1, respectively.

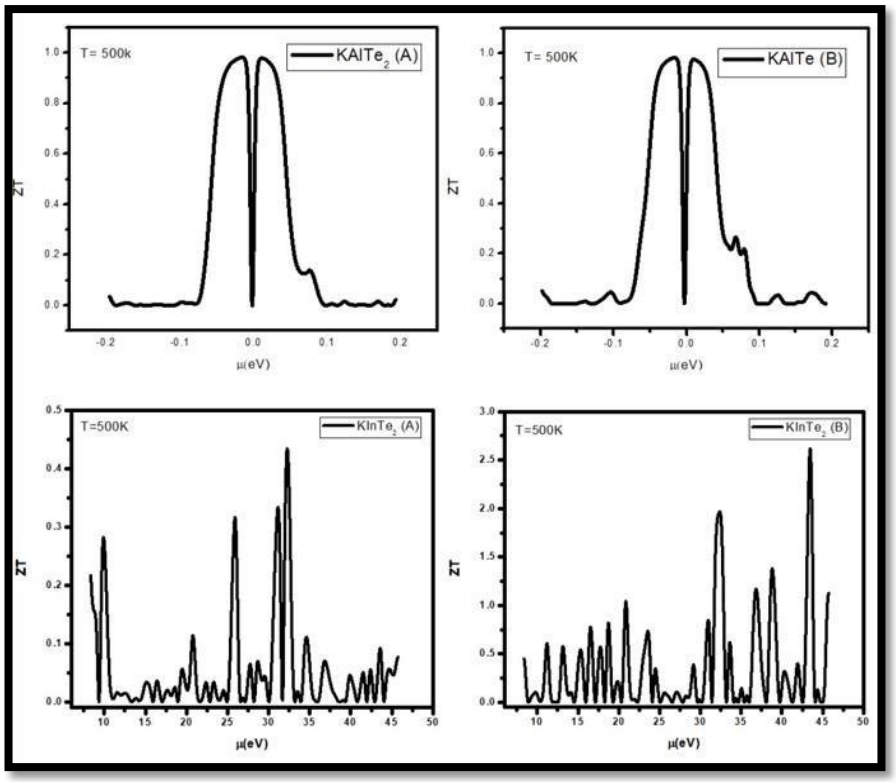

Figure 6(a, b): the figure of merit for $KAlTe_2$ and $KInTe_2$ as a function of the chemical potential

Clearly, according to the data presented, all the analyzed compounds exhibit a commendable level of efficiency for thermoelectric applications. Notably, the ZT values for both $KAlTe_2$ and $KInTe_2$ exceed 1, signifying the material's suitability for thermoelectric purposes due to its favorable thermal performance.

4. Conclusion

In the present research analysis, we used DFT to analyze the electronic and thermoelectric characteristics of the tetragonal materials $KAlTe_2$ and $KInTe_2$. The material possesses a tetragonal crystal structure, and experimental data were utilized to study its covalent bonding. Materials known for their high stability and anisotropy were subjected to DFT analyses. At their respective extremes, both materials exhibit brittleness and ductility, making them crucial in the field of materials science. The energy of each compound is minimized to achieve the ground state, with the objective of enhancing the structural properties of these materials. The findings are contrasted with prior experimental and theoretical observations. Both of the materials reported are identified as indirect band gap semiconductors, with reference to the Γ and R points. The calculated band gaps for $KAlTe_2$ and $KInTe_2$ using this approach are 1.68 eV and 0.931 eV, respectively. The primary reason for the numerical decrease in the band gap is the substitution of Al atoms with in atoms. $KAlTe_2$ exhibits paramagnetic behavior, whereas $KInTe_2$ displays diamagnetic characteristics. The findings are contrasted with prior experimental and theoretical observations. Both of the materials under investigation are identified as indirect band gap semiconductors, with reference to the Γ and R points. The calculated band gaps for $KAlTe_2$ and $KInTe_2$ using this approach are 1.68 eV and 0.931 eV, respectively.

Reference

Baira, M., Siad, A. B., & Siad, M. (2021). A new investigation of Ruddlesden-Popper compounds Ba2MO4 (M= Sn, Pb) through structural, elastic, electronic, optical and thermoelectric properties. *Journal of Solid State Chemistry, 294*, 121843.

Belgoumri, G., Bentabet, A., Khenata, R., Bouhadda, Y., Benmakhlouf, A., Rai, D., . . . Bounab, S. (2018). Insight into the structural, electronic and elastic properties of AInQ2 (A: K, Rb and Q: S, Se, Te) layered structures from first-principles calculations. *Chinese journal of physics, 56*(3), 1074-1088.

Benmakhlouf, A., Bentabet, A., Bouhemadou, A., Maabed, S., Khenata, R., & Bin-Omran, S. (2015). Structural, elastic, electronic and optical properties of KAlQ2 (Q= Se, Te): A DFT study. *Solid State Sciences, 48*, 72-81.

Benmekideche, N., Bentabet, A., Bouhadda, Y., Boubatra, D., Belgoumri, G., Fetah, S., . . . Benyelloul, K. (2018). DFT study of structural, electronic and elastic properties of two polymorphs of monoclinic CsGaQ2 (Q= S, Se). *Chinese journal of physics, 56*(3), 1345-1352.

Bouchenafa, M., Benmakhlouf, A., Sidoumou, M., Bouhemadou, A., Maabed, S., Halit, M., . . . Al-Douri, Y. (2020). Theoretical investigation of the structural, elastic, electronic, and optical properties of the ternary tetragonal tellurides KBTe2 (B= Al, In). *Materials Science in Semiconductor Processing, 114*, 105085.

Claeys, C., Hsu, P.-C., Mols, Y., Han, H., Bender, H., Seidel, F., . . . Waldron, N. (2020). Electrical Activity of Extended Defects in Relaxed InxGa1− xAs Hetero-Epitaxial Layers. *ECS Journal of Solid State Science and Technology, 9*(3), 033001.

Dipsey, M. J. (2016). *Working towards a normally off GaN based MOSHEMT*: Lehigh University.

Fabiano, E., Constantin, L. A., & Sala, F. D. (2011). Exchange-correlation generalized gradient approximation for gold nanostructures. *The Journal of chemical physics, 134*(19).

Feng, S., Wang, N., Li, M., Xiao, H., Liu, Z., Zu, X., & Qiao, L. (2021). The thermal and electrical transport properties of layered LaCuOSe under high pressure. *Journal of Alloys and Compounds, 861*, 157984.

Feng, Y., Zhang, J., Qin, P., Liu, S., Yang, Q., Meng, J., . . . Xie, J. (2019). Characterization of elevated-temperature high strength and decent thermal conductivity extruded Mg-Er-Y-Zn alloy containing nano-spaced stacking faults. *Materials Characterization, 155*, 109823.

Fu, Y., Duan, X., Xing, M., Zhang, N., Luo, X., Wang, H., & Ma, Y. (2014). Low-temperature synthesis of NaInS2 nanoplate layered structure by one-step solvothermal decomposition of In (S2CNEt2) 3 complex. *Materials Letters, 124*, 141-143.

Gerolin, A., Grossi, J., & Gori-Giorgi, P. (2019). Kinetic correlation functionals from the entropic regularization of the strictly correlated electrons problem. *Journal of Chemical Theory and Computation, 16*(1), 488-498.

Gori-Giorgi, P., & Baerends, E. J. (2018). Asymptotic nodal planes in the electron density and the potential in the effective equation for the square root of the density. *The European Physical Journal B, 91*, 1-10.

Hardianto, H. (2020). *Textile-based thermoelectric generators based on conductive yarns.* Ghent University,

Hausmann, J., Oudah, M., Ikeda, A., Yonezawa, S., & Maeno, Y. (2018). Controlled synthesis of the antiperovskite oxide superconductor Sr3− xSnO. *Superconductor Science and Technology, 31*(5), 055012.

Ikeda, A., Koibuchi, S., Kitao, S., Oudah, M., Yonezawa, S., Seto, M., & Maeno, Y. (2019). Negative ionic states of tin in the oxide superconductor Sr 3− x SnO revealed by Mössbauer spectroscopy. *Physical Review B, 100*(24), 245145.

Isaenko, L., Vasilyeva, I., Merkulov, A., Yelisseyev, A., & Lobanov, S. (2005). Growth of new nonlinear crystals LiMX2 (M= Al, In, Ga; X= S, Se, Te) for the mid-IR optics. *Journal of crystal growth, 275*(1-2), 217-223.

Isaenko, L., Yelisseyev, A., Lobanov, S., Titov, A., Petrov, V., Zondy, J. J., . . . Smirnova, J. (2003). Growth and properties of LiGaX2 (X= S, Se, Te) single crystals for nonlinear optical applications in the mid-IR. *Crystal Research and Technology: Journal of Experimental and Industrial Crystallography, 38*(3-5), 379-387.

Kaur, T., & Sinha, M. (2021). *Probing thermoelectric properties of high potential Ca3PbO: An Ab Initio Study.* Paper presented at the IOP Conference Series: Materials Science and Engineering.

Kim, J., & Hughbanks, T. (2000). Synthesis and structures of ternary chalcogenides of aluminum and gallium with stacking faults: KMQ2 (M= Al, Ga; Q= Se, Te). *Journal of Solid State Chemistry, 149*(2), 242-251.

March, N. H., & Angilella, G. G. (2016). *Exactly solvable models in many-body theory*: World Scientific.

Mardirossian, N., & Head-Gordon, M. (2016). ωB97M-V: A combinatorially optimized, range-separated hybrid, meta-GGA density functional with VV10 nonlocal correlation. *The Journal of chemical physics, 144*(21).

Moltved, K. A., & Kepp, K. P. (2019). The metal hydride problem of computational chemistry: Origins and consequences. *The Journal of Physical Chemistry A, 123*(13), 2888-2900.

Morrison, R. A. (2019). *Equations of State, Sound Velocities, and Thermoelasticity of Iron-Nickel-Silicon Alloys in the Earth's Inner Core*: California Institute of Technology.

Perdew, J. P., Ruzsinszky, A., Csonka, G. I., Vydrov, O. A., Scuseria, G. E., Constantin, L. A., . . . Burke, K. (2008). Restoring the density-gradient expansion for exchange in solids and surfaces. *Physical review letters, 100*(13), 136406.

Range, K., & Mahlberg, G. (1975). High pressure transformations of the alkali thioindates KInS 2, RbInS 2 and CsInS 2. *Z. Naturforsch., B, 30*(1), 81-87.

Saeed, M., Ali, A., Haq, I. U., Muhammad, S., Chaudhry, A. R., ur Rehman, A., . . . Khan, I. (2022). First-principles study of the structural and optoelectronic properties of ANbO3 (A= Na, K and Rb) in four crystal phases. *Materials Science in Semiconductor Processing, 139*, 106364.

Saeed, M., Haq, I. U., Saleemi, A. S., Rehman, S. U., Haq, B. U., Chaudhry, A. R., & Khan, I. (2022). First-principles prediction of the ground-state crystal structure of double-perovskite halides Cs2AgCrX6 (X= Cl, Br, and I). *Journal of Physics and Chemistry of Solids, 160*, 110302.

Saeed, M., Khan, B., Ahmad, I., Saleemi, A. S., Rehman, N., Aliabad, H. R., & Uddin, S. (2019). Theoretical investigations of thermoelectric phenomena in binary semiconducting skutterudites. *RSC advances, 9*(43), 24981-24986.

Saeed, M., Noor, Z., Laref, A., Althib, H., Flemban, T. H., & Murtaza, G. (2021). Insights into the structural, electronic and optical properties of MgA2B4 (A= Sc, Y; B= S, Se) spinel compounds: direct energy band gap materials. *Materials Science in Semiconductor Processing, 127*, 105736.

Saeed, M., Uddin, W., Ali, S., Saleemi, A. S., Khan, K., Rehman, S. U., & Khan, M. (2021). Structural, electronic, optical and thermoelectric analysis of perovskites xruo3 (x= ca, sr). *Physica B: Condensed Matter, 614*, 412962.

Schubert, H., & Hoppe, R. (1970). Zur Kenntnis der RbInS2-Strukturfamilie. *Zeitschrift für Naturforschung B, 25*(8), 886-887.

Sofi, A., & Shah, M. (2019). Structural and electrical properties of copper doped In2O3 nanostructures prepared by citrate gel processes. *Materials Research Express, 6*(4), 045039.

Ward, M. D., Pozzi, E. A., Van Duyne, R. P., & Ibers, J. A. (2014). Syntheses, structures, and optical properties of the indium/germanium selenides Cs4In8GeSe16, CsInSe2, and CsInGeSe4. *Journal of Solid State Chemistry, 212*, 191-196.

Weis, J., Schäfer, H., & Schön, G. (1976). Neue ternäre Telluride und Selenide der Alkalimetalle mit Elementen der 3. Hauptgruppe. New Ternary Element (I)/Element (III)-Tellurides and Selenides. *Zeitschrift für Naturforschung B, 31*(10), 1336-1340.

Xiaoying, D. (2020). NUMERICAL METHODS AND THEORIES FOR ELECTRONIC STRUCTURE CALCULATIONS. *Mathematica Numerica Sinica, 42*(2), 131.

Xie, Q.-X., Wu, J., & Zhao, Y. (2021). Accurate correlation energy functional for uniform electron gas from an interpolation ansatz without fitting parameters. *Physical Review B, 103*(4), 045130.

Yuan, X., Sun, Y., Guo, H., Shi, K., Song, P., Han, H., . . . Li, L. (2021). Design of negative/nearly zero thermal expansion behavior over a wide temperature range by multi-phase composite. *Materials & Design, 203*, 109591.